Materials Characterization 144 (2018) 411–423

Contents lists available at ScienceDirect

Materials Characterization

journal homepage: www.elsevier.com/locate/matchar

# Grain boundary inter-connections in polycrystalline aluminum with random orientation

Weiguo Wang[a,d,*], Changhui Cai[a], Gregory S. Rohrer[b], Xinfu Gu[c], Yan Lin[a,d], Song Chen[a,d], Pinqiang Dai[a,d]

[a] School of Materials Science and Engineering, Fujian University of Technology, Fuzhou 350118, China
[b] Department of Materials Science and Engineering, Carnegie Mellon University, Pittsburgh, PA 15213-3890, USA
[c] School of Materials Science and Engineering, University of Science and Technology Beijing, Beijing 100083, China
[d] Fujian Provincial Key Laboratory of Advanced Materials Processing and Application, Fuzhou 350118, China

ARTICLE INFO

*Keywords:*
Aluminum
Grain boundary inter-connection
Electron backscatter diffraction
Five parameter analysis

ABSTRACT

Grain boundary inter-connection (GBIC) is the matching of two crystallographic planes from two abutting grains ending on the grain boundary (GB) position in polycrystalline materials, which can be expressed as $\{h_1\ k_1\ l_1\}/\{h_2\ k_2\ l_2\}$. GBIC is the critical parameter that intrinsically defines the character and properties of a GB. In current work, a zone-melted polycrystalline aluminum bar with a purity higher than 99.99% (mass fraction) was subjected to a multi-directional forging (MDF) with a true strain of 4 followed by a recrystallization annealing at 360 °C. Such process repeated at least 4 times until an equiaxed-grain microstructure with random orientation and averaged grain size approximate 30 μm was achieved. Then the GBICs were determined by electron backscatter diffraction (EBSD) measurement and stereology-based five-parameter analysis (FPA) coupled with crystallographic analysis after the grain boundaries (GBs) were filtered according to their misorientations (e.g. angle/axis pair). The results revealed that the GBICs for any group of GBs with a given misorientation are not random, showing remarkable preference on the planes of low Miller index forming mixed and twist GBs. The work also demonstrated that among the high angle boundaries (HABs), {1 1 1}/{1 1 1}, including coherent Σ3 boundaries, is the most frequent GBIC, mainly due to the GBs formed by rotations around ⟨1 1 1⟩, ⟨1 2 2⟩ and ⟨1 1 2⟩ axes. Near coincidence site (NCS) and O-lattice theory analyses indicate that the {1 1 1}/{1 1 1} GBICs usually possess higher planar coincidence site density (PCSD) and definite dislocation structures compared to the general GBs, implying their more structural stability when only crystallography is taken into account. This result agrees very well with the recent results obtained by molecular dynamic simulations. It is significant to the grain boundary engineering (GBE) in the high stacking fault energy (SFE) face-centered cubic (FCC) materials such as aluminum and its alloys.

## 1. Introduction

Grain boundary (GB) is an essential structure unit [1,2] and always plays a crucial role in the manipulation of the microstructure as well as the manipulation of the varied properties in polycrystalline materials. Usually, the GBs are classified into low angle boundaries (LABs) and high angle boundaries (HABs), whose misorientation angles are lower than 10° and greater than 15°, respectively. The GBs are also divided into twist, tilt and mixed types in which the rotation axes are parallel, perpendicular and heterotropic to the GB normal, respectively. A LAB can be treated in the frame of dislocation theories and its structure has a definite relationship with the misorientation as Frank-Bilby [3,4] formulized. Owing to their slight deviations from the ideal crystal, the LABs usually possess a higher degree of atomic ordering and thus higher structural stability. Hence, LABs are generally regarded as special or singular boundaries. However, in the case of HABs, the situation turns to be more complicated. The structure of a HAB cannot be dealt with just in terms of dislocation theories. This is the reason why the GB anisotropy is still an open question, and it indeed turns to be a tough barrier in the simulations [5,6] of microstructural evolution in polycrystalline materials. In the history of scientific investigations concerning the structure and character of HABs, the issue of coincidence site lattice (CSL) GB which was proposed by Kronberg and Wilson [7] in their investigation into the secondary recrystallization in copper was a

* Corresponding author at: School of Materials Science and Engineering, Fujian University of Technology, Fuzhou 350118, China.
*E-mail address:* wang_weiguo@vip.163.com (W. Wang).

https://doi.org/10.1016/j.matchar.2018.07.040
Received 2 May 2018; Received in revised form 25 June 2018; Accepted 31 July 2018
Available online 02 August 2018
1044-5803/ 

step of mile-stone. The most recognized contributions of CSL-GB is that it stimulated the research interest upon the relationship between GB structure and GB properties for the HABs [8], leading to the emerge of grain boundary engineering (GBE) or in other words the optimization of grain boundary character distribution (GBCD) which was proposed by Watanabe [9]. He stated that the CSL-GBs with Σ value no > 29 are special boundaries, and the overall properties of the material may be improved substantially if the frequency and spatial distributions of such boundaries were controlled reasonably by a proper thermal mechanical processing (TMP). Since electron backscatter diffraction (EBSD) was put into commercial application in 1993 [10], a huge number of GBE investigations have been carried out in a variety of materials including austenitic stainless steel [11–13], lead-calcium based alloys [14–16], nickel based super alloys [17–19] and brass [20,21]. The GB related properties especially the intergranular corrosion resistance have been dramatically improved.

However, the CSL theory is not an almighty measure and some other approaches must be considered for the treatments of structure-property correlations of HABs. The reasons may be summarized into the following three points. (1) The CSL GBs only cover very limited HABs corresponding to some specific misorientations, it cannot be able to smooth every corners of the structural-relevant issues of HABs in overall. (2) Nearly all of the GBE researches in the past were aimed at the low to medium stacking fault energy (SFE) face-centered cubic (FCC) metals. The GBCD evolution of such metals in the GBE processing are dominated by a so called twin-induced mechanism [22,23] in which strain-induced boundary migration (SIBM) [24,25] introduces a huge quantity of Σ3 boundaries (twin boundaries) in the materials through the interactions between migrating boundaries and strained matrix, and the resultant GBCD contains a high frequency Σ3 boundaries and its family generations such as Σ9 and Σ27 boundaries. Thus, it is naturally questioned that what is the point-cut into the GBE research and GBCD control in high SFE FCC metals such as aluminum and its alloys, body-centered cubic (BCC) and even hexagonal close packed (HCP) metals because only a few (usually < 5% out of the entire GBs) $\Sigma 3^n$ (n = 1,2,3) and other low Σ (Σ ≤ 29) CSL boundaries can be achieved in these metals. (3) The GBCDs are generally characterized based on EBSD measurement in which the character of each GB is determined according to the GB misorientations which involves only three independent parameters, usually the axis/angle pair (e.g. [u v w]/θ, in which only two of the three parameters of the rotation axis [u v w] are independent ones). It is only reasonable for the twin-induced GBE as the authors previously argued [26]. These three points suggest that, for a general investigation into the structure-property correlations of HABs, especially for the GBE research and application of high SFE-FCC, BCC and even HCP structured metals, some other approaches including the measurements of grain boundary plane distribution (GBPD) [26,27] and the analysis of grain boundary inter-connection (GBIC) [28,29] must be considered and applied. The GBPD measurement involves five independent parameters (The misorientation in angle-axis pair contains three parameters as mentioned above, GB normal orientation in the crystallographic frame gives another two), which can be determined by the three dimensional method of serial sectioning [30,31]. However, the most efficient and simple method is the stereology and statistics based five parameter analysis (FPA) [32,33], which enables us to obtain a GBPD result of statistical significance after collecting the data by EBSD just from any single section of a sample. The GBIC analysis is realized by crystallographic analysis based on the GBPD of the GBs with the same misorientation, which is readily screened through a GB filtration. So far, compared with misorientation and GBPD, GBIC is the most reasonable parameter that defines the character of a GB. GBIC will be generally applicable to the GBE research in any type of materials.

A GBIC means the coupling of two crystallographic planes from the two abutting grains terminating on the grain boundary position in polycrystalline materials, which can be expressed as $\{h_1\ k_1\ l_1\}/\{h_2\ k_2\ l_2\}$ corresponding to the Miller indexes of the two inter-connected crystallographic planes. It was referred to by Pumphreys [34], Randle [35] and Palumbo [36]. Although it may be argued that in the atomistic scale the $\{h_1\ k_1\ l_1\}/\{h_2\ k_2\ l_2\}$ seems meaningless because the atoms are not located on the exact lattice position due to the relaxation caused by the irregular crystal-field potential in the GB region, averagely it is reasonable and it dominates the atomic configurations in a GB region such as the dislocation structure (usually the secondary dislocation structure), the shape and size of free volume, the faceting mode and even the precipitation behaviors [37–40]. Another argument may be aroused from the fact that in some cases the GBs are curved, and thus the GBIC expression is not applicable. This is true in the case that the material is heat-treated at an elevated temperature during which the GBs are highly excited and driven to migrate rapidly, usually leading to a rough and curved GB morphology [24]. But in the most cases the GBs are flat type and the GBIC definition is acceptable, and this is always the case for a well recrystallized microstructure in metals and ceramics. Therefore, GBIC is a critical and general parameter which is the point-cut of next-step GBE research. In fact, the twin-induced GBE researches as mentioned above were using GBIC knowingly. The reason is that over 60% out of the entire $\Sigma 3^n$ (n = 1, 2, 3) boundaries are the coherent twin boundaries, which are real-special and having the {1 1 1}/{1 1 1} GBIC. It is always right just to use misorientation-based three parameters to characterize the GBCDs when the frequency of $\Sigma 3^n$ (n = 1, 2, 3) boundaries reaching approximately 80% out of the entire boundaries, because in this condition, the frequency of real special (coherent twin) boundaries approaches 50% out of the entire boundaries and the GB related performance is improved dramatically. In other words, the GBCD control in the twin-induced GBE is actually a {1 1 1}/{1 1 1} GBIC control. Another point that may be emphasized is that the GBIC should be closely correlated with the grain boundary complexion [41–43] in which a phase-transformation-like mutation of GB character is highlighted. This is just the case in the microstructure evolution during which the GB annihilation, GB regeneration and GB reconstruction (two separate moving GBs join into one) take place frequently, and it certainly leads to the GBIC reconstruction. Moreover, once the GBIC is determined, it is easy to use the O-lattice theory [44,45] to figure out the dislocation structures and thus to make contributions to the issue of GB anisotropy.

So, GBIC is an intrinsic parameter in polycrystalline materials. GBIC determination is not only crucial to the GBE researches, but also important to the microstructure manipulation and thus property manipulation which relies on the cooperative behaviors of each GB in the three dimensional GB networks. Since both chemical composition and crystallographic texture have substantial effects on the surface energy of the crystallographic planes and thus have effects on the GBPDs [46,47] and GBICs, high purity polycrystalline aluminum with random orientation will be used in the current work to study the GBIC. The results will be helpful in understanding the intrinsic GBCD configuration in pure aluminum, and thus significant to the GBE research in high SFE FCC metals.

## 2. Experimental Procedure

### 2.1. Materials and Treatments

Zone-melted high purity aluminum (99.99%, mass fraction) was used as experimental material. A sample with a size of 50 mm × 25 mm × 25 mm was cut from the mother bar and then subjected to a multi-directional forging (MDF) at room temperature. The forging procedure is schematically shown in Fig. 1. The true strain ε can be determined according to the following formalism

$$\varepsilon = \ln(h_1/h_2) \quad (1)$$

where $h_1$ and $h_2$ is the height of the sample before and after forging in any direction (e.g. x or y or z direction as shown in Fig. 1), respectively. The height reduction of forging in any direction is set to be 50%,

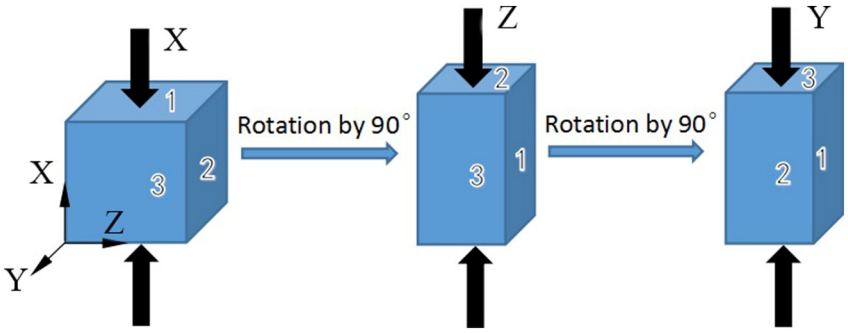


**Fig. 1.** Schematic illustration of multi-directional forging (MDF).

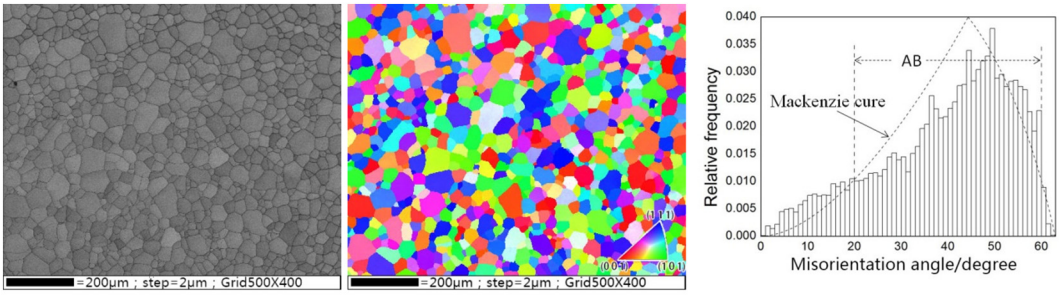


**Fig. 2.** Microstructure of the pure aluminum sample as processed. (a) EBSD band contrast (BC) map; (b) orientation imaging microscopy (OIM); (c) misorientation distribution of grain boundaries.

namely ($h_2/h_1$) = 0.5. One cycle MDF includes the forgings in the x, y and z three directions and the true strain in total is 2. In current work, the sample was given a two-cycle MDF followed by a recrystallization annealing at 360 °C, and such treatment was repeated for 4 times to achieve a uniform microstructure as shown in Fig. 2. It can be seen that the grain size in the as-processed sample is considerably even and the averaged grain size is approximately 30 μm (Fig. 2a), the grain orientations are fairly random and no distinct crystallographic textures are observed in the orientation imaging microscopy (OIM) (Fig. 2b), and the misorientation profile (Fig. 2c) is in good agreement with Mackenzie [48] curve indicating again the random orientation of the grains. Additionally, it can also be seen that the microstructure of the sample as-processed is fully recrystallized, showing the GBs in straight lines in the EBSD band contrast (BC) map (Fig. 2a) and OIM (Fig. 2b), implying the flat-type morphology of GBs. Such a microstructure with an even grain size, random orientation and flat-type GBs is exactly expected in the current work as mentioned in the foregoing text in the section of introduction.

### 2.2. Measurement of GBPD

The GBPD measurement includes the steps of EBSD sample preparation, EBSD data collection, GB segment extraction, GB filtration and GBPD determination.

EBSD sample preparation includes the procedures of mechanical polishing and electro-chemical polishing. A small sample in a size of 10 mm × 8 mm × 1.3 mm which was cut by a high precision saw (Beuhler EM 5000) from the bigger sample as processed was mechanically polished by emery paper. Then the sample was subjected to an electro-chemical polishing in an ice-cooled solution of perchloric acid:ethanol = 1:9 (volume fraction) at 20 V for 4 min. After this two-step polishing, the sample with a mirror-like surface was obtained and ready for EBSD data collection.

EBSD data collection was realized by using an Oxford Aztec facility attached to a FEI Nova nano 450 field emission scanning electron microscope (FE-SEM). During the data collection, the SEM and EBSD working parameters were set to an acceleration voltage of 20 kV, spot size of 4.5, working distance of 9 mm and step size of 2 μm. The frame size for each EBSD mapping was 1000 μm × 800 μm. In order to ensure the results to be statistical significance, several tens of EBSD mappings were taken from the sample so that the number of GBs was > 50,000. After data collection, lot of information such as BC grain morphology, OIM, GB misorientations and so on were obtained through data processing. The crystallographic information of GBs was achieved by the GB segment extraction.

The GB segment extraction was finished by the TSL 5.0 software taking the OIM as input data. It was a two-dimensional processing in which each GB segment was identified and fixed by comparing the Euler angles pixel by pixel. After this processing, all the information such as the start and end point coordinates of each GB in the sample frame, the length of each GB, the Euler angles of the two grains abutted by each GB and the ID number were achieved.

GB filtration was realized by a small code composed by the authors. The GB segments as obtained above were taken as input data in this processing, and the GB misorientations were obtained by a simple calculation [49] incorporating the two sets of Euler angles of the two grains bounded by each GB. During the calculation, the GB misorientations were reduced into the fundamental zone of Rodrigus-Frank space [50]. Hence, the maximum rotation angle was 62.8° corresponding to the ⟨1 1 √2-1⟩ rotation axis when the GB misorientation was expressed by angle/axis pair. The filtration was finished via two separate steps, namely the axis filtration and angular filtration. The axis filtration was filtering the GBs according to their rotation axes with an angular resolution of 5°, and the rotation axes were limited to the low Miller index ones including ⟨0 0 1⟩, ⟨0 1 1⟩, ⟨1 1 1⟩, ⟨0 1 2⟩, ⟨1 1 2⟩, ⟨1 2 2⟩, ⟨0 1 3⟩ and ⟨1 1 3⟩. The angular filtration was filtering the GBs according to their misorientation angles for the GBs with given rotation axis filtered as above. As HABs were the main concern in the current work, the GBs with misorientation angles ranging from 20° to 60° were emphasized. During angular filtration, angular interval and angular

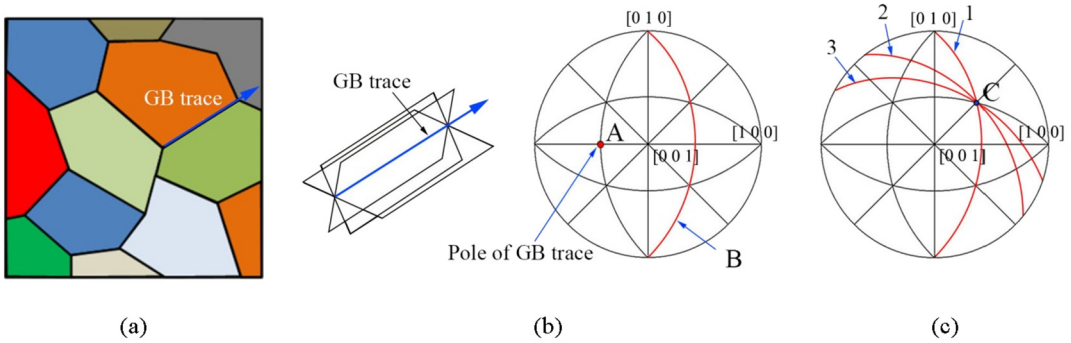


**Fig. 3.** Schematic illustration of five parameter analysis (FPA) method. (a) OIM map and the grain boundary (GB) trace; (b) (0 0 1) projection of the GB trace and the large circle B of possible orientation of GB plane; (c) three GB traces derived large circles intersecting one point C indicating the most probable GB plane orientation.

resolution were set to be 5° and 2.5°, respectively. For explicit, the filtered GBs with a misorientation of ⟨0 0 1⟩/25° means a group of GBs with misorientations ranging from ⟨0 0 1⟩/22.5° to ⟨0 0 1⟩/27.5°.

The GBPD was determined by the FPA method [32,33] as mentioned in the introduction section. Concerning this method, some points needs to be emphasized. (1) The crystallographic orientations of the GB traces (GB segments) (Fig. 3a) revealed by the OIMs were calculated based on the data obtained in the procedure of GB segment extraction. (2) The probable orientation of each GB plane, namely the orientation of the normal of each GB plane in the crystallographic frame was determined according the theory of stereology. As shown in Fig. 3b, which is a projection of three dimensional (3D) crystallographic orientations onto the (0 0 1) (two dimensional, 2D) where A is the orientation of a GB trace. Then the probable orientation of the GB plane must be located in the large circle B, whose zone is just the GB trace A. Briefly, in the five parameters which exactly decide the geometry of a GB plane, the misorientation between any two abutted grains gives the first three, the crystallographic orientation of GB trace gives the fourth and the fifth must be located in the large circle of which its zone is just the GB trace. (3) The GBPD of statistical significance for any group of GBs with a given misorientation as filtered above was assessed by counting the large circle numbers passing through each orientation bin. For example, supposing there are three GB segments of which the corresponding large circles are 1, 2 and 3, respectively, as labeled in Fig. 3c and these three large circles are all passing through the orientation bin C, then it arrives at a result that the GB planes (or the GB plane normal) are most probably oriented in the orientation bin C. According to stereology, it is usually using length fraction of GB segments as obtained in OIM to represent the area fraction of GB planes in three dimensional (3D) GB networks. The GBPD intensity in a certain orientation can be determined by the function $\lambda(\Delta g, n)$ in which $\Delta g$ means the misorientation between the two adjacent grains and $n$ the orientation of grain boundary plane in the crystallographic coordinate. The general expression of $\lambda(\Delta g, n)$ is

$$\lambda(\Delta g, n) = \frac{l_i^c}{<l^o>} \tag{2}$$

$$l_i^c = \frac{l_i^{oc} + (Z-1)\frac{(D-1)}{D} < l^o>}{1 + Z(D-1)} \tag{3}$$

$$l_i^{oc} = \sum_{j=1}^{m} \frac{l_{ij}^o}{q_{ij}} \tag{4}$$

where the subscript $i$ means the $i$th orientation bin in the top semisphere of crystallographic space, $l_i^c$ is the true value of GB segment length summed to the $i$th orientation bin, $< l^o >$ is the observed mean value of GB segment length in each orientation bin, $D$ is the bin numbers in 0°–90°, $Z$ is a fraction of concentric circles around the bin of interest that falls within an angular range of π/2, then Z = 2/$D$, so $< l^o > /D$ is the actual mean value of GB segment length in each orientation bin in the case of random distribution, and $\lambda(\Delta g, n)$ is the multiples of random distribution (MRD); $m$ is the observed number of GB segments of which the large circle of GB plane normal pass through the $i$th orientation bin, and $l_{ij}^o$ is the observed length of the $j$th GB segment; $q_{ij}$ is an intensity factor of crystallographic texture of the $j$th grain boundary segment, and $l_i^{oc}$ is the observed grain boundary length after crystallographic texture correction; As mentioned above, $\lambda(\Delta g, n)$ is usually projected onto a specific crystallographic plane such as (0 0 1) for cubic and this projection is referred to GBPD. The actual GBPD determination is more sophisticated, which needs a large number of GB segments and involves the statistical principles and stereology theory and the detailed descriptions can be referred to the papers published elsewhere [32,33,51].

### 2.3. Determination of GBIC

The GBIC is usually determined by the GBs of a given misorientation $[u\ v\ w]/\theta$ ($[u\ v\ w]$ is the rotation axis and $\theta$ is the rotation angle) based on the GBPDs, and the following equation [52] is essential.

$$\begin{bmatrix} h_2 \\ k_2 \\ l_2 \end{bmatrix} = \mathrm{R}_{[u\ v\ w]/\theta} \begin{bmatrix} h_1 \\ k_1 \\ l_1 \end{bmatrix} \tag{5}$$

$$\mathrm{R}_{[u\ v\ w]/\theta} = \begin{bmatrix} u^2(1-\cos\theta)+\cos\theta & uv(1-\cos\theta) - w\sin\theta & uw(1-\cos\theta) + v\sin\theta \\ uv(1-\cos\theta) + w\sin\theta & v^2(1-\cos\theta) + \cos\theta & vw(1-\cos\theta) - u\sin\theta \\ uw(1-\cos\theta) - v\sin\theta & vw(1-\cos\theta) + u\sin\theta & w^2(1-\cos\theta) + \cos\theta \end{bmatrix} \tag{6}$$

where ($h_1$ $k_1$ $l_1$) is one of the intensity peak positions which can be ascertained directly on the GBPD, $\mathrm{R}_{[u\ v\ w]/\theta}$ is the misorientation matrix relevant to the given misorientation $[u\ v\ w]/\theta$ in which $u$, $v$ and $w$ is normalized as $u^2 + v^2 + w^2 = 1$, and ($h_2$ $k_2$ $l_2$) is derived from Eq. (5). If ($h_2$ $k_2$ $l_2$) is also one of the intensity peak positions on the GBPD, it is believed that there is a GBIC of ($h_1$ $k_1$ $l_1$)/($h_2$ $k_2$ $l_2$). Obviously all the GBICs can be determined according to Eqs. (5) and (6) if the GBs of any given misorientation are taken into consideration one by one. Of course, it should be noted that only when the intensity is > 1.10 MRD on the GBPD, the corresponding planes could be considered as GBIC relevant. The GBIC results given in current work are qualitative though the processing involves statistical treatment.

**Table 1**
The components of GBs as filtered.

| GB rotation axes | 0 0 1 | 0 1 1 | 1 1 1 | 0 1 2 | 1 1 2 | 1 2 2 | 0 1 3 | 1 1 3 |
|---|---|---|---|---|---|---|---|---|
| Length fraction, % | 1.7 | 12.3 | 15.9 | 9.9 | 15.9 | 26.6 | 8.0 | 9.7 |
| GB numbers | 281 | 1923 | 2399 | 1569 | 2546 | 4217 | 1270 | 1570 |

## 3. Results

### 3.1. GB Components Determined by GB Filtration

Over 55,000 GB segments are identified and extracted from the OIMs developed from 25 EBSD mappings. As only those GBs having the rotation axes with low Miller index including ⟨0 0 1⟩, ⟨0 1 1⟩, ⟨1 1 1⟩, ⟨0 1 2⟩, ⟨1 1 2⟩, ⟨1 2 2⟩, ⟨0 1 3⟩ and ⟨1 1 3⟩ will be considered in current work, there are 15,775 GB segments left after GB filtration according to their rotation axes with an angular resolution of 5°. These GBs are divided into eight components in terms of GB rotation axes, as listed Table 1, giving the information of length fraction as well as numbers for each component. Two remarkable features can be seen in Table 1. One is ⟨0 1 1⟩, ⟨1 1 1⟩, ⟨1 1 2⟩ and ⟨1 2 2⟩ GB components constitute the main part and take up nearly three fourths (over 70%) of the total GBs as filtered. The other is ⟨0 0 1⟩ GB takes up a very low fraction, which gives a striking contrast compared to the result as the authors obtained in BCC structured pure iron [51].

The GB components listed in Table 1 are further filtered according to their misorientation angles ranging from 5° to 60° with an angular interval of 5° and an angular resolution of 2.5°. Fig. 4 shows the relative frequencies versus misorientation angles for each GB component. For a clear comparison it also shows the relative frequencies of some low Σ CSL boundaries (the shaded rectangular). Concerning Fig. 4, two points need to be stressed. One is the truncated misorientation angle is different from one GB component to another, for example it is 45° for ⟨0 0 1⟩ and ⟨0 1 3⟩ GB components while it is 50° for ⟨0 1 2⟩ and ⟨1 1 3⟩ GB components, which depends on the geometry of the fundamental zone of Rodrigus space [50]. The other is the averaged misorientation-distribution envelopment of the eight GB components is in good accordance with the Mackenzie cure as observed in Fig. 2c. Since the GBs with misorientation angles lower than 15° are those LABs which are always termed as special boundaries, only those HABs with misorientation angles higher than 20° (section AB as indicated in Fig. 2c) will be considered in current work.

### 3.2. GBPDs of the GBs of Given Misorientations

Since the ⟨0 1 1⟩, ⟨1 1 1⟩, ⟨1 1 2⟩ and ⟨1 2 2⟩ GB components constitute the main part of the GBs as filtered (Table 1), their GBPDs will be focused and emphasized and it is significant for us to understand the characteristics of the GBPDs and the GBICs of major aspects. Fig. 5 gives the GBPDs of the GBs of given misorientations for ⟨1 1 1⟩ GB component. It is clear that all the GBPDs dramatically deviate from the random distribution, showing intensity peaks on some specific crystallographic planes whereas most frequently on {1 1 1}, indicating that there is a preference on {1 1 1} for the GB plane orientations during recrystallization. The same phenomenon can be seen in the GBPDs of ⟨1 2 2⟩ and ⟨1 1 2⟩ GB components, as shown in Figs. 6 and 7. It may be relevant to the fact that the directions of ⟨1 1 2⟩ and ⟨1 2 2⟩ are very close to ⟨1 1 1⟩. Concerning this point some discussions will be made hereafter in the Section 4. However, as shown in Fig. 8 the GBPDs of the ⟨0 1 1⟩ GB component are quite different from that observed in the ⟨1 1 1⟩ one, though there are some intensity peaks on {1 1 1}. It indicates that the GBPDs intrinsically correlate with the rotation axes of GB misorientations. Additionally, some particular features can be seen from the GBPDs of ⟨0 0 1⟩ GB component as shown Fig. 9.

### 3.3. GBICs of the GBs of Given Misorientations

Based on the GBPDs and formulas (5) and (6) as given above, it is easy to determine the GBICs for the GBs of given misorientations. Taking Fig. 5a for example, the intensity peaks are appearing on {1 1 1}, {2 2 3} and {0 1 1}, and for the specific misorientation [1 1 1]/20° (note: Fig. 5a corresponds to a given misorientation ⟨1 1 1⟩/20°, including four specific misorientations such as [1 1 1]/20°, [−1 1 1]/20°, [−1 −1 1]/20° and [1 −1 1]/20°. They are crystallographic identical), its misorientation matrix is given as following

$$R_{[1\,1\,1]/20^{o}} = \begin{bmatrix} 0.9598 & -0.1774 & 0.2176 \\ 0.2176 & 0.9598 & -0.1774 \\ -0.1774 & 0.2176 & 0.9598 \end{bmatrix} \tag{7}$$

If let $(h_1\ k_1\ l_1)$ be (1 1 1), (−3 −2 2) and (0 1 1), by using formulas (5)–(7), we can get $(h_2\ k_2\ l_2)$ is (1 1 1), (−2.08954 −2.92703 2.01654) ≈ (−2 −3 2) and (0.04021 0.78244 1.17737) ≈ (0 2 3), respectively. Therefore, it is found that the GBICs for the GBs with the specific misorientation [1 1 1]/20° are (1 1 1)/(1 1 1), (−3 −2 2)/(−2 −3 2) and (0 1 1)/(0 2 3) (Fig. 5a). Since the other intensity peaks as shown in Fig. 5a are appearing on the planes crystallographic identical to (1 1 1) or (2 2 3) or (0 2 3), it is easy to determine that the GBICs in

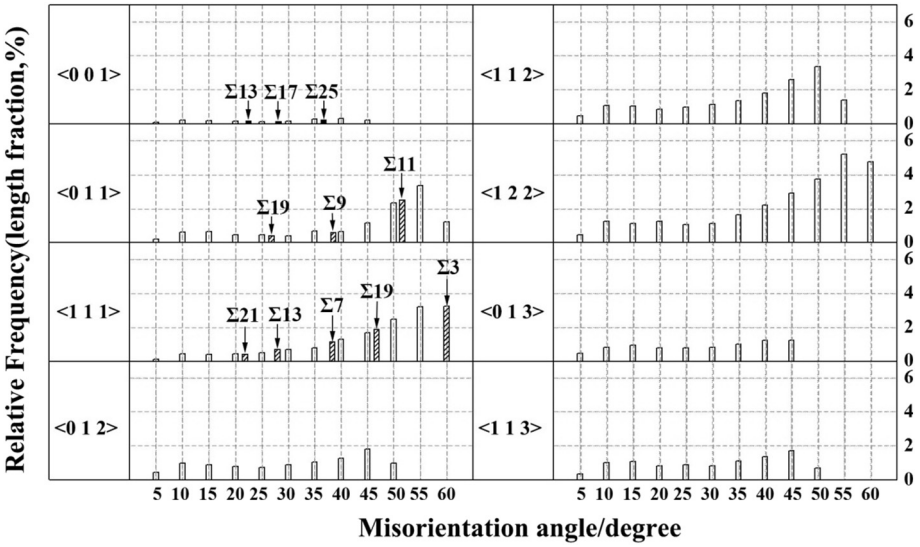


**Fig. 4.** Relative frequency versus misorientation angle for each GB component after GB filtration.

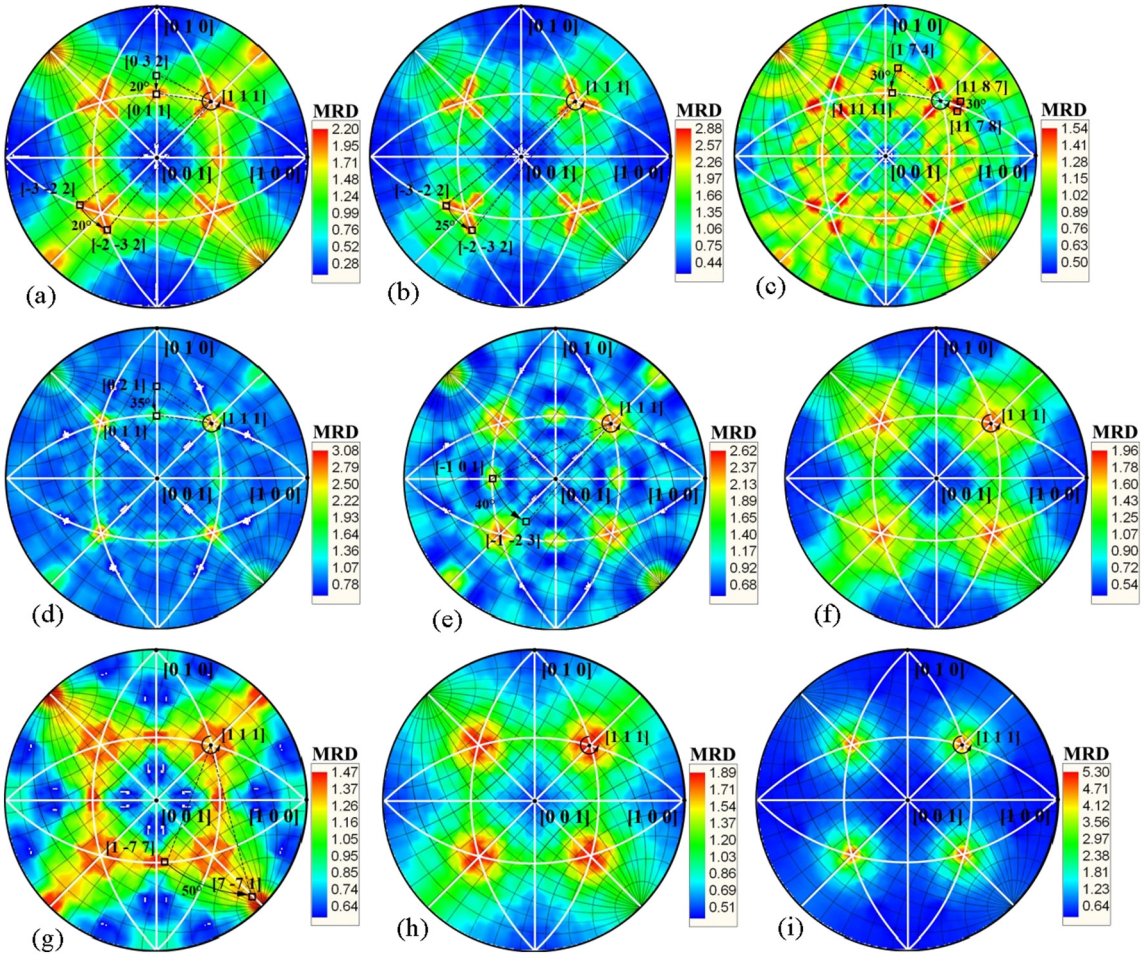


**Fig. 5.** Grain boundary plane distributions (GBPD) of the ⟨1 1 1⟩ GB component (projected onto (0 0 1)).
(a)–(i) corresponding to [111]/20°, [1 1 1]/25°, [1 1 1]/30°, [1 1 1]/35°, [1 1 1]/40°, [1 1 1]/45°, [1 1 1]/50°, [1 1 1]/55° and [1 1 1]/60°, respectively.

general for the GBs with the given misorientation ⟨1 1 1⟩/20° are {1 1 1}/{1 1 1}, {2 2 3}/{2 2 3} and {0 1 1}/{0 2 3}. Here, it may be emphasized that the weaker intensity of {0 2 3} does not affect the formation of {0 1 1}/{0 2 3} GBIC. The reason is the multiplicity factor of {0 2 3} is twice as that of {0 1 1}. By the same way, the GBICs of other GBs with given misorientations (Fig. 5b–i) of ⟨1 1 1⟩ GB component are determined. All GBICs observed in ⟨1 1 1⟩ GB component are summarized in Table 2, and in regard to this table, two points need to be stressed. One is the exact ($h_2$ $k_2$ $l_2$) values calculated based on the misorientation matrix and formulas (5)–(6) with ($h_1$ $k_1$ $l_1$) value being integers are usually non-integers, they are all reduced into integers in a rational deviation. The other is the rotations relevant to the GB misorientations are all counter-clockwise when determining ($h_2$ $k_2$ $l_2$) with rotation axes and ($h_1$ $k_1$ $l_1$) fixed, as shown in Fig. 5. Similarly, the GBICs developed in ⟨1 2 2⟩, ⟨1 1 2⟩, ⟨0 1 1⟩ and ⟨0 0 1⟩ GB components are determined and briefly summarized in Table 3.

(a)~(f) corresponding to [001]/20°, [0 0 1]/25°, [0 0 1]/30°, [0 0 1]/35°, [0 0 1]/40°, [0 0 1]/45°, respectively.

## 4. Discussions

### 4.1. Characteristics of GBPDs and GBICs

As can be seen from Figs. 5 to 9, the GBPDs of the GBs with any given misorientation are not random, showing remarkable preference on some crystallographic planes especially on the low Miller index planes. This may be explained by Rohrer's work [53] in which it found that the population of GB planes in the GBPD is inversely proportional to their surface energy, planes of lower Miller index usually possess lower surface energy, hence larger population in the GBPD. The current work agrees very well with that result [53]. Specially, in FCC structured materials, the closely packed planes {1 1 1} have the lowest surface energy according to Wulff [54], thus they should averagely be the most frequent ones among the observed planes in the GBPDs. This is also in a very good accordance with the current work. Another point should be emphasized is that the rotation axes related to the misorientations of the GBs is one more kernel factor on the GBPDs. As shown in Figs. 8–9, the GB planes of ⟨0 1 1⟩ and ⟨0 0 1⟩ GB components are rarely appearing on {1 1 1}, giving a strike contrast to that of ⟨1 1 1⟩, ⟨1 2 2⟩ and ⟨1 1 2⟩ GB components. This could be attributed to bulk geometrical constraint, whose nature needs to be explored further. Anyway, the small population of {1 1 1} developed in ⟨0 1 1⟩ and ⟨0 0 1⟩ GB components doesn't affect the averaged GBPDs because the major parts of the GBs come from ⟨1 1 1⟩, ⟨1 2 2⟩ and ⟨1 1 2⟩ GB components (Table 1).

From Figs. 5–9 and Tables 2–3, we can also see that the GBICs of the GBs with any given misorientation are not random and the two planes of the GBICs are also appeared to be low Miller indexed ones averagely. The most remarkable feature of the GBICs as observed is that most of the two inter-connected planes of the GBICs are having identical Miller indexes, namely {$h_1$ $k_1$ $l_1$} = {$h_2$ $k_2$ $l_2$}, forming twist, mixed or tilt GBs. Since it not only depends on the combined behaviors of two inter-connected planes, but also closely related to recrystallization nucleation and grain growth in which the very complicated GB reconstruction resulting from the three dimensional (3D) GB network evolution [55,56] must be considered, the underlying formation mechanism of

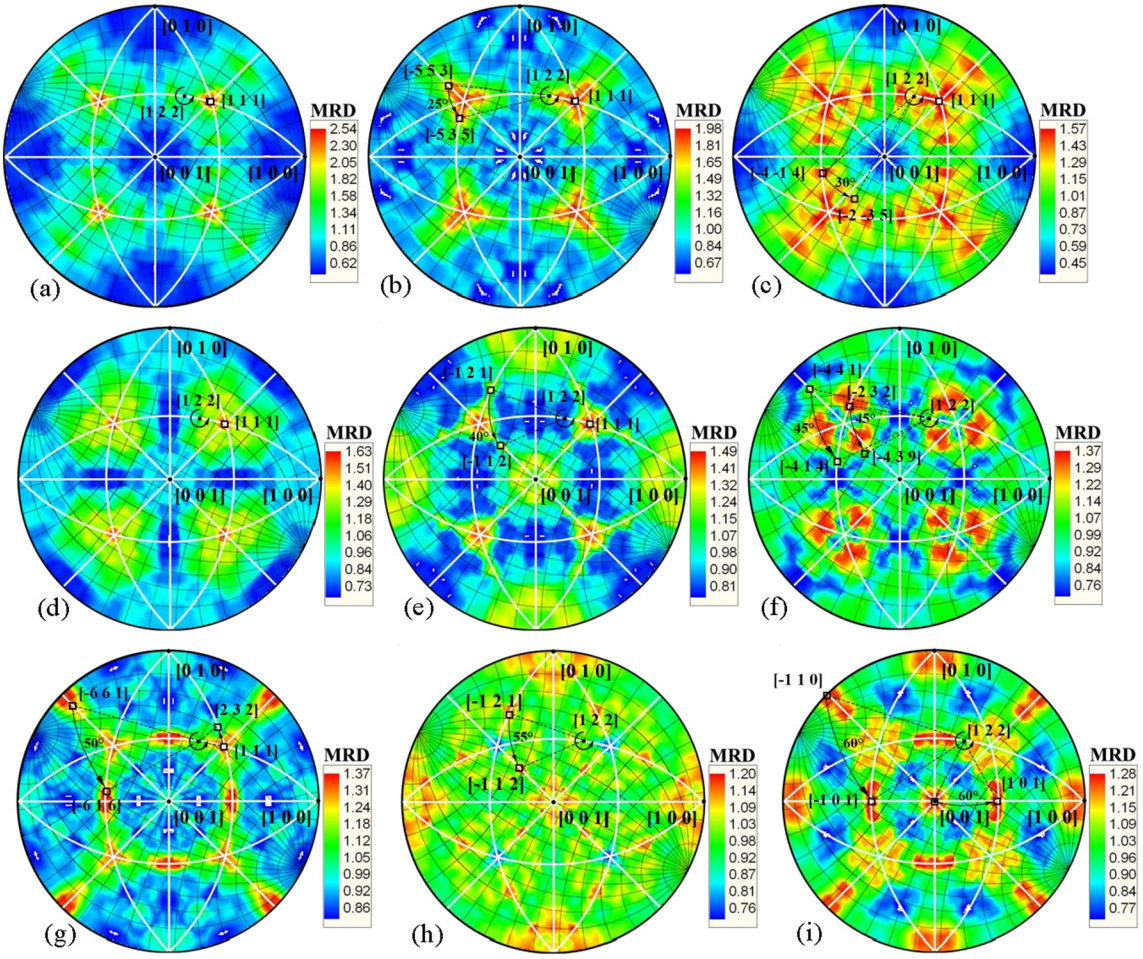


**Fig. 6.** Grain boundary plane distributions (GBPD) of the ⟨1 2 2⟩ GB component (projected onto (0 0 1)).
(a)–(i) corresponding to [1 2 2]/20°, [1 2 2]/25°, [1 2 2]/30°, [1 2 2]/35°, [1 2 2]/40°, [1 2 2]/45°, [1 2 2]/50°, [1 2 2]/55°, [1 2 2]/60°, respectively.

the GBICs is still an open question. The only reasonable explanation for the observed GBICs is that all the GBICs are approaching to a state of lower energy or to a state which is in favor of the progressing towards a lower energy state of bulk microstructure.

### 4.2. GB Types and Their Frequencies

Revisiting Figs. 5–9 and Tables 1–3, it is easy to find that, although there have developed three types of GBs (twist, mixed and tilt types) in the material, the frequency of the GBs is different from one type to another and it is obviously related to the rotation axes of the misorientations. As shown in Table 2, among the 16 GBs (GBICs specific) observed in ⟨1 1 1⟩ GB component, half of them are twist type, 6 are mixed type and only 2 are tilt type. However, no twist GBs are observed in the ⟨0 1 1⟩ GB component and nearly all of the GBs are mixed type in ⟨1 2 2⟩ and ⟨1 1 2⟩ GB components (Table 3). If the (1 1 1)/(1 1 1) GBs (GBICs specific) as observed in the ⟨1 2 2⟩ and ⟨1 1 2⟩ GB components are approximated into ⟨1 1 1⟩ twist type based on the fact of small intersection angle between [1 2 2] or [1 1 2] and [1 1 1], it is found that the frequency of twist GBs are much higher than that of tilt ones. This result indicates again the twist GBs are structurally more stable than the tilt ones, which must be correlated with the intrinsic dislocation structures or atomic configurations [57,58] in the two type GBs.

One more point needs to be stressed is that the frequencies of the low Σ (Σ ≤ 29) [9] CSL GBs is generally not higher compared to that of random GBs. As shown in Fig. 4, the frequencies of Σ7 (⟨1 1 1⟩/38.21°) and Σ17 (⟨0 0 1⟩/28.07°) are not higher than that of the nearby random GBs such as ⟨1 1 1⟩/40° and ⟨0 0 1⟩/30°, respectively. Even the frequency of Σ3 (⟨1 1 1⟩/60°) GBs is just a little bit higher than that of the nearby random GB (⟨1 1 1⟩/55°). The same phenomenon can be seen in the comparison between other low Σ CSL GBs and their nearby random GBs as indicated in Fig. 4. This should be the intrinsic characteristics of the high purity aluminum which possesses high SFE with FCC structure. It is quite different from the low to medium SFE FCC materials in which very high frequent low Σ CSL GBs, especially Σ3 and its family Σ9 and Σ27 GBs can be introduced during annealing after deformation [59–62].

### 4.3. The Most Frequent GBIC

It is estimated that the most frequent GBIC as observed in current work is {1 1 1}/{1 1 1}, including all ⟨1 1 1⟩ twist GBs from the ⟨1 1 1⟩ GB component and those approximated from the ⟨1 2 2⟩ and ⟨1 1 2⟩ GB components. This estimation is based on the following three points.

(1) In the ⟨0 1 1⟩, ⟨1 1 1⟩, ⟨1 2 2⟩ and ⟨1 1 2⟩ four GB components which constitute the main part of the GBs as filtered (Table 1), just to consider the ⟨1 1 1⟩, ⟨1 2 2⟩ and ⟨1 1 2⟩ three components is rational because they take over 80% out of these four components. To ignore the contributions from ⟨0 1 1⟩ GB component will not substantially affect the results, let alone the GBICs as observed in this component are so scattered (Fig. 8 and Table 3).
(2) In the ⟨1 1 1⟩ GB component, except the GBs with the misorientation ⟨1 1 1⟩/30°, the other GBs with misorientations ranging from ⟨1 1 1⟩/20° to ⟨1 1 1⟩/60° are all having {1 1 1}/{1 1 1} GBIC (Fig. 5 and Table 2), indicating there is a very high content of {1 1

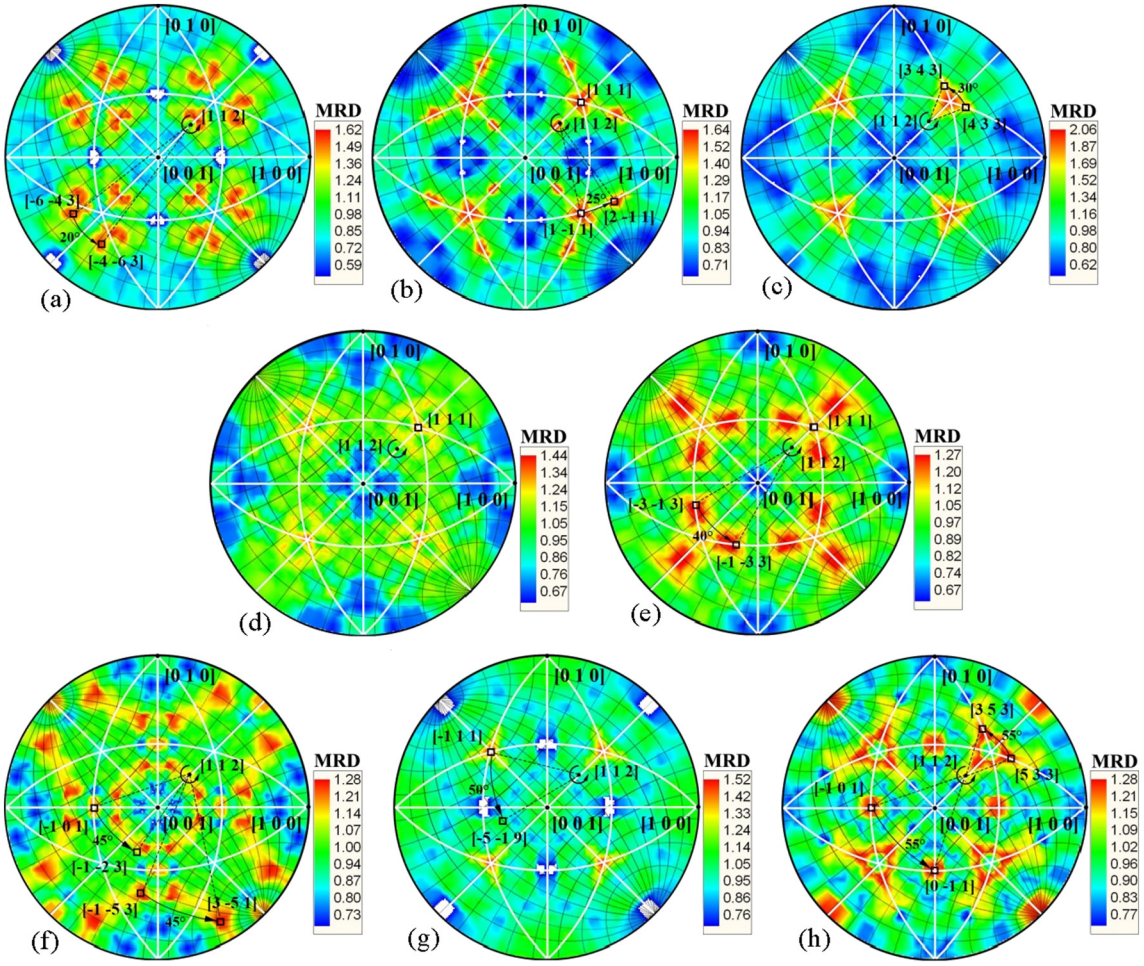


**Fig. 7.** Grain boundary plane distributions (GBPD) of the ⟨1 1 2⟩ GB component (projected onto (0 0 1)).
(a)–(h) corresponding to [1 1 2]/20°, [1 1 2]/25°, [1 1 2]/30°, [1 1 2]/35°, [1 1 2]/40°, [1 1 2]/45°, [1 1 2]/50°, [1 1 2]/55°, respectively.

1}/{1 1 1} GBIC, namely the most frequent GBIC is {1 1 1}/{1 1 1} in ⟨1 1 1⟩ GB component.

(3) In the ⟨1 2 2⟩ GB component, {1 1 1}/{1 1 1} GBICs exist in the GBs with misorientations ranging from ⟨1 1 1⟩/20° to ⟨1 1 1⟩/40° (Fig. 6 and Table 3). Although this is not an exact determination, it is a reasonable estimation. The reason is the intersection angle between [1 2 2] and [1 1 1] is only 15.8° (Fig. 10), planes deviate ± 5.4° from the exact (1 1 1) position are covered by a rotation operation around [1 2 2] for 20° (from 0° to 20° or from 20° to 40°) and within this range the plane having the smallest Miller index is (10 11 9), which is anyway can be approximated into (1 1 1). The same estimation can be made on the ⟨1 1 2⟩ GB component because the intersection angle between [1 1 2] and [1 1 1] is 19.5°, a little bit greater than that between [1 2 2] and [1 1 1]. Hence, when tuning back to Table 3 and Figs. 6–7, it is easy to find {1 1 1}/{1 1 1} is the most frequent GBIC in the ⟨1 2 2⟩ and ⟨1 1 2⟩ GB components.

Based on the three points mentioned above, it is reasonable that the most frequent GBIC observed in current work is {1 1 1}/{1 1 1}. It implies {1 1 1}/{1 1 1} could be structurally the most stable GBIC apart from the coherent twin boundaries. This result not only agrees very well with the recent computational results reported by Janssens et al. [63] who found that the mobility of all {1 1 1}/{1 1 1} interconnected GBs is much lower compared to that of the GBs of other types, but also keeps consistence with the early results [64,65] in which it claimed the GBs formed by the planes of larger inter-planar spacing are usually more resistant to precipitations of impurities implying their more structural stability.

### 4.4. The Atomic Structure of {1 1 1}/{1 1 1} GBIC

As {1 1 1}/{1 1 1} is the most frequent GBIC observed in current work, it is necessary to learn about its atomic structures. The conventional method such as transmission electron microscopy (TEM) needs to know the exact misorientation before observing the atomic structures of a GB under high resolution mode, this leads to too much uneasiness, and sometimes no result can be obtained because of the thin area limit of a foil specimen. Therefore, the computer simulation method is used in current work to configure the atomic structures of the {1 1 1}/{1 1 1} GBIC. Fig. 11 shows the schematic illustrations of atomic structures of some {1 1 1}/{1 1 1} GBICs relevant to ⟨1 1 1⟩ GB component. These figures are plotted based on the near coincident sites (NCS) frame [66] in which the NCS criterion is set to be 0.10a (a is the lattice parameter). It can be seen the planar coincidence site density (PCSD) for the four {1 1 1}/{1 1 1} GBICs in Fig. 11 is 1.27/nm$^2$, 1.08/nm$^2$, 1.20/nm$^2$ and 1.20/nm$^2$, respectively. They are remarkably higher than that of the general random GBs, whose PCSD is usually lower than 0.5/nm$^2$ when same NCS criterion is used. This result indicates that the {1 1 1}/{1 1 1} GBICs could be more stable compared with the general random GBs if only crystallography is considered.

For further consideration, O-lattice theory [45] is used to figure the dislocation structures in {1 1 1}/{1 1 1} GBICs. Taking the [1 1 1]/45° misoriented (1 1 1)/(1 1 1) GBIC for example, the nearby CSL

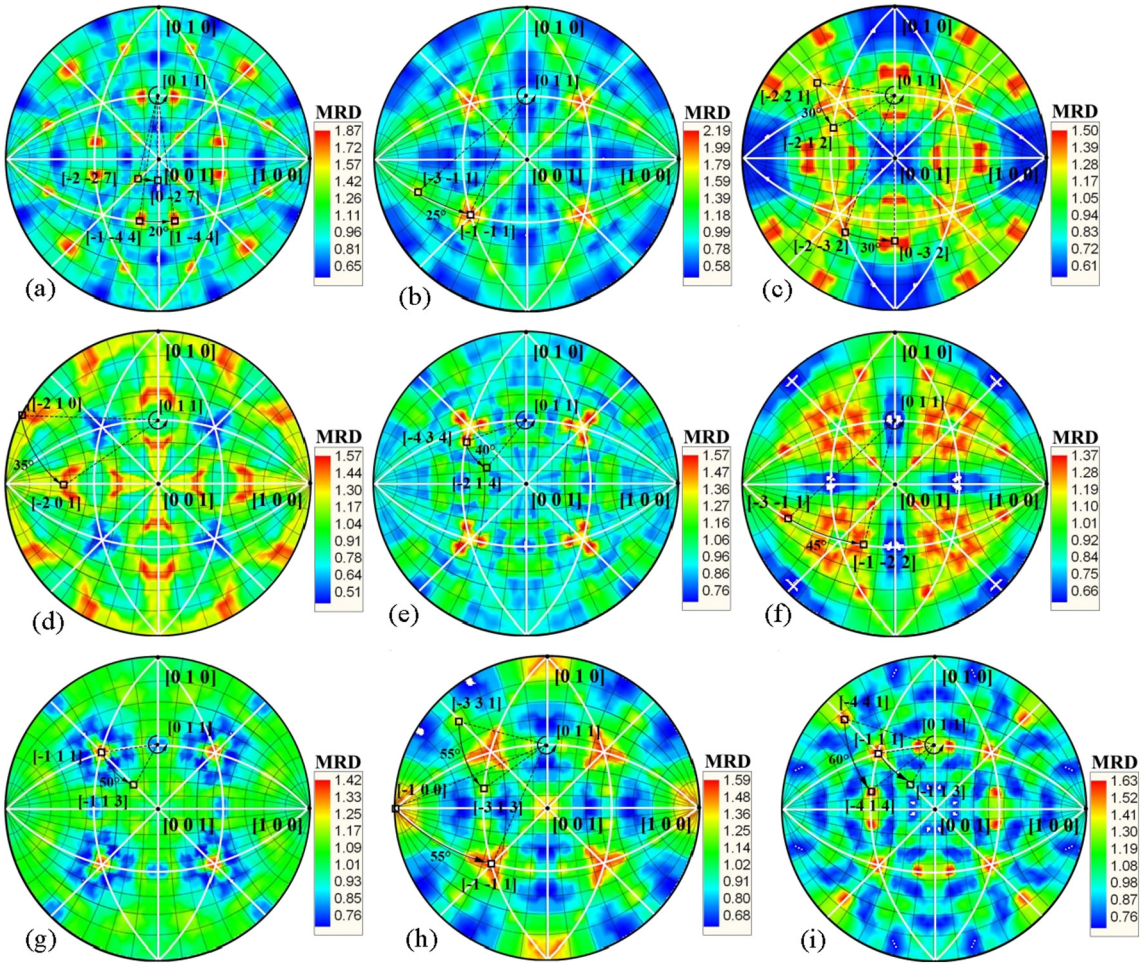


**Fig. 8.** Grain boundary plane distributions (GBPD) of the ⟨0 1 1⟩ GB component (projected onto (0 0 1)).
(a)–(i) corresponding to [0 1 1]/20°, [0 1 1]/25°, [0 1 1]/30°, [0 1 1]/35°, [0 1 1]/40°, [0 1 1]/45°, [0 1 1]/50°, [0 1 1]/55°, [0 1 1]/60°, respectively.

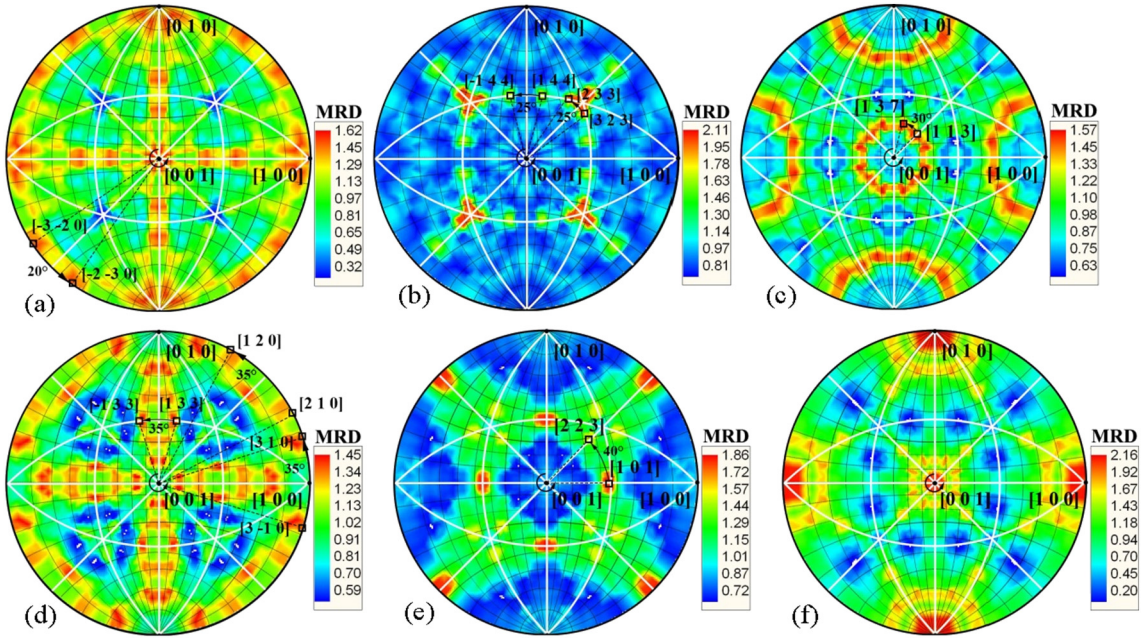


**Fig. 9.** Grain boundary plane distributions (GBPD) of the ⟨0 0 1⟩ GB component (projected onto (0 0 1)).

**Table 2**
The GBICs of the ⟨1 1 1⟩ GB component.

| Misorientations | Misorientation matrix | GBICs | Misorientations | GBICs |
|---|---|---|---|---|
| (Specific) | (Specific) | (Specific) | (General) | (General) |
| [1 1 1]/20° | $\begin{bmatrix} 0.9598 & -0.1774 & 0.2176 \\ 0.2176 & 0.9598 & -0.1774 \\ -0.1774 & 0.2176 & 0.9598 \end{bmatrix}$ | (1 1 1)/(1 1 1)<br>(−3 −2 2)/(−2 −3 2)<br>(0 1 1)/(0 2 3) | ⟨1 1 1⟩/20° | {1 1 1}/{1 1 1}<br>{2 2 3}/{2 2 3}<br>{0 1 1}/{0 2 3} |
| [1 1 1]/25° | $\begin{bmatrix} 0.9375 & -0.2128 & 0.2752 \\ 0.2752 & 0.9375 & -0.2128 \\ -0.2128 & 0.2752 & 0.9375 \end{bmatrix}$ | (1 1 1)/(1 1 1)<br>(−3 −2 2)/(−2 −3 2) | ⟨1 1 1⟩/25° | {1 1 1}/{1 1 1}<br>{2 2 3}/{2 2 3} |
| [1 1 1]/30° | $\begin{bmatrix} 0.9107 & -0.2440 & 0.3333 \\ 0.3333 & 0.9107 & -0.2440 \\ -0.2440 & 0.3333 & 0.9107 \end{bmatrix}$ | (11 7 8)/(11 8 7)<br>(1 7 4)/(1 11 11) | ⟨1 1 1⟩/30° | {7 8 11}/{7 8 11}<br>{1 4 7}/{1 11 11} |
| [1 1 1]/35° | $\begin{bmatrix} 0.8794 & -0.2709 & 0.3914 \\ 0.3914 & 0.8794 & -0.2709 \\ -0.2709 & 0.3914 & 0.8794 \end{bmatrix}$ | (1 1 1)/(1 1 1)<br>(0 1 1)/(0 1 2) | ⟨1 1 1⟩/35° | {1 1 1}/{1 1 1}<br>{0 1 1}/{0 1 2} |
| [1 1 1]/40° | $\begin{bmatrix} 0.8440 & -0.2931 & 0.4491 \\ 0.4491 & 0.8440 & -0.2931 \\ -0.2931 & 0.4491 & 0.8440 \end{bmatrix}$ | (1 1 1)/(1 1 1)<br>(−1 0 1)/(−1 −2 3) | ⟨1 1 1⟩/40° | {1 1 1}/{1 1 1}<br>{0 1 1}/{1 2 3} |
| [1 1 1]/45° | $\begin{bmatrix} 0.8047 & -0.3106 & 0.5059 \\ 0.5059 & 0.8047 & -0.3106 \\ -0.3106 & 0.5059 & 0.8047 \end{bmatrix}$ | (1 1 1)/(1 1 1) | ⟨1 1 1⟩/45° | {1 1 1}/{1 1 1} |
| [1 1 1]/50° | $\begin{bmatrix} 0.7619 & -0.3232 & 0.5614 \\ 0.5614 & 0.7619 & -0.3232 \\ -0.3232 & 0.5614 & 0.7619 \end{bmatrix}$ | (1 1 1)/(1 1 1)<br>(−1 0 1)/(−1 −4 5) | ⟨1 1 1⟩/50° | {1 1 1}/{1 1 1}<br>{0 1 1}/{1 4 5} |
| [1 1 1]/55° | $\begin{bmatrix} 0.7157 & -0.3308 & 0.6151 \\ 0.6151 & 0.7157 & -0.3308 \\ -0.3308 & 0.6151 & 0.7157 \end{bmatrix}$ | (1 1 1)/(1 1 1) | ⟨1 1 1⟩/55° | {1 1 1}/{1 1 1} |
| [1 1 1]/60° | $\begin{bmatrix} 0.6667 & -0.3333 & 0.6667 \\ 0.6667 & 0.6667 & -0.3333 \\ -0.3333 & 0.6667 & 0.6667 \end{bmatrix}$ | (1 1 1)/(1 1 1) | ⟨1 1 1⟩/60° | {1 1 1}/{1 1 1} |

**Table 3**
The GBICs of ⟨1 2 2⟩, ⟨1 1 2⟩, ⟨0 1 1⟩ and ⟨0 0 1⟩ GB components.

| Misorientations | GBICs | Misorientations | GBICs | Misorientations | GBICs | Misorientations | GBICs |
|---|---|---|---|---|---|---|---|
| (Specific) | (Specific) | (General) | (General) | (Specific) | (Specific) | (General) | (General) |
| [1 2 2]/20° | (1 1 1)/(1 1 1) | ⟨1 2 2⟩/20° | {1 1 1}/{1 1 1} | [1 1 2]/20° | (2 2 3)/(2 2 3) | ⟨1 1 2⟩/20° | {2 2 3}/{2 2 3} |
| [1 2 2]/25° | (1 1 1)/(1 1 1)<br>(−5 5 3)/(−5 3 5) | ⟨1 2 2⟩/25° | {1 1 1}/{1 1 1}<br>{3 5 5}/{3 5 5} | [1 1 2]/25° | (1 1 1)/(1 1 1)<br>(1 1 2)/(1 1 2) | ⟨1 1 2⟩/25° | {1 1 1}/{1 1 1}<br>{1 1 2}/{1 1 2} |
| [1 2 2]/30° | (1 1 1)/(1 1 1)<br>(−1 −4 4)/(4 −10 7) | ⟨1 2 2⟩/30° | {1 1 1}/{1 1 1}<br>{1 4 4}/{4 7 10} | [1 1 2]/30° | (1 1 1)/(1 1 1)<br>(4 3 3)/(3 4 3) | ⟨1 1 2⟩/30° | {1 1 1}/{1 1 1}<br>{3 3 4}/{3 3 4} |
| [1 2 2]/35° | (1 1 1)/(1 1 1) | ⟨1 2 2⟩/35° | {1 1 1}/{1 1 1} | [1 1 2]/35° | (1 1 1)/(1 1 1) | ⟨1 1 2⟩/35° | {1 1 1}/{1 1 1} |
| [1 2 2]/40° | (1 1 1)/(1 1 1)<br>(−1 2 1)/(−1 1 2) | ⟨1 2 2⟩/40° | {1 1 1}/{1 1 1}<br>{1 1 2}/{1 1 2} | [1 1 2]/40° | (1 1 1)/(1 1 1)<br>(6 5 6)/(5 6 6) | ⟨1 1 2⟩/40° | {1 1 1}/{1 1 1}<br>{5 6 6}/{5 6 6} |
| [1 2 2]/45° | (−2 3 2)/(−4 3 9)<br>(−4 4 1)/(−4 1 4) | ⟨1 2 2⟩/45° | {2 2 3}/{3 4 9}<br>{1 4 4}/{1 4 4} | [1 1 2]/45° | (−1 0 1)/(−1 −2 3)<br>(−1 −5 3)/(3 −5 1) | ⟨1 1 2⟩/45° | {0 1 1}/{1 2 3}<br>{1 3 5}/{1 3 5} |
| [1 2 2]/50° | (1 1 1)/(2 3 2)<br>(−1 0 1)/(−1 −7 12) | ⟨1 2 2⟩/50° | {1 1 1}/{2 2 3}<br>{0 1 1}/{1 7 12} | [1 1 2]/50° | (−1 −1 1)/(1 −5 2) | ⟨1 1 2⟩/50° | {1 1 1}/{1 2 5} |
| [1 2 2]/55° | (−1 2 1)/(−1 1 2) | ⟨1 2 2⟩/55° | {1 1 2}/{1 1 2} | [1 1 2]/55° | (−1 0 1)/(0 −1 1)<br>(5 3 3)/(3 5 3) | ⟨1 1 2⟩/55° | {0 1 1}/{0 1 1}<br>{3 3 5}/{3 3 5} |
| [1 2 2]/60° | (−1 1 0)/(−1 0 1)<br>(0 1 0)/(−5 8 6) | ⟨1 2 2⟩/60° | {0 1 1}/{0 1 1}<br>{0 0 1}/{5 6 8} | [1 1 2]/60° | NA | ⟨1 1 2⟩/60° | NA |
| [0 1 1]/20° | (−1 −4 4)/(1 −4 4)<br>(−2 −2 7)/(0 −2 7) | ⟨0 1 1⟩/20° | {1 4 4}/{1 4 4}<br>{2 2 7}/{0 2 7} | [0 0 1]/20° | (0 0 1)/(0 0 1)<br>(−2 3 0)/(−3 2 0) | ⟨0 0 1⟩/20° | {0 0 1}/{0 0 1}<br>{0 2 3}/{0 2 3} |
| [0 1 1]/25° | (−3 −1 1)/(−1 −1 1) | ⟨0 1 1⟩/25° | {1 1 3}/{1 1 1} | [0 0 1]/25° | (3 2 3)/(2 3 3)<br>(1 4 4)/(−1 4 4) | ⟨0 0 1⟩/25° | {1 1 3}/{1 1 1}<br>{1 4 4}/{1 4 4} |
| [0 1 1]/30° | (−2 −3 2)/(0 −3 2)<br>(−2 2 1)/(−2 1 2) | ⟨0 1 1⟩/30° | {2 2 3}/{0 2 3}<br>{1 2 2}/{1 2 2} | [0 0 1]/30° | (1 1 3)/(1 3 7) | ⟨0 0 1⟩/30° | {1 1 3}/{1 3 7} |
| [0 1 1]/35° | (−2 1 0)/(−2 0 1) | ⟨0 1 1⟩/35° | {0 1 2}/{0 1 2} | [0 0 1]/35° | (−1 2 0)/(−2 1 0)<br>(−3 1 0)/(−3 −1 0)<br>(1 3 3)/(−1 3 3) | ⟨0 0 1⟩/35° | {0 1 2}/{0 1 2}<br>{0 1 3}/{0 1 3}<br>{1 3 3}/{1 3 3} |
| [0 1 1]/40° | (−4 3 4)/(−2 1 4) | ⟨0 1 1⟩/40° | {3 4 4}/{1 2 4} | [0 0 1]/40° | (1 0 1)/(2 2 3) | ⟨0 0 1⟩/40° | {0 1 1}/{2 2 3} |
| [0 1 1]/45° | (−3 −1 1)/(−1 −2 2) | ⟨0 1 1⟩/45° | {1 1 3}/{1 2 2} | [0 0 1]/45° | (0 0 1)/(0 0 1)<br>(−2 1 1)/(−2 −1 1) | ⟨0 0 1⟩/45° | {0 0 1}/{0 0 1}<br>{1 1 2}/{1 1 2} |
| [0 1 1]/50° | (−1 1 1)/(−1 1 3) | ⟨0 1 1⟩/50° | {1 1 1}/{1 1 3} | [0 0 1]/50° | NA | ⟨0 0 1⟩/50° | NA |
| [0 1 1]/55° | (−1 0 0)/(−1 −1 1)<br>(−3 3 1)/(−3 −1 3) | ⟨0 1 1⟩/55° | {0 0 1}/{1 1 1}<br>{1 3 3}/{1 3 3} | [0 0 1]/55° | NA | ⟨0 0 1⟩/55° | NA |
| [0 1 1]/60° | (−4 4 1)/(−4 1 4)<br>(−1 1 1)/(−1 1 3) | ⟨0 1 1⟩/60° | {1 4 4}/{1 4 4}<br>{1 1 1}/{1 1 3} | [0 0 1]/60° | NA | ⟨0 0 1⟩/60° | NA |

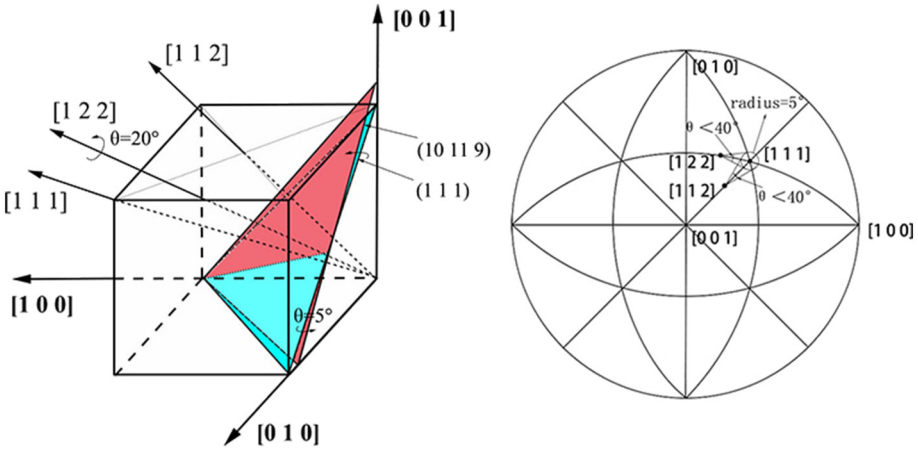


**Fig. 10.** Schematic illustration of crystallography of (1 1 1) and (10 11 9) relevant to the rotation around [1 2 2] and [1 1 2].

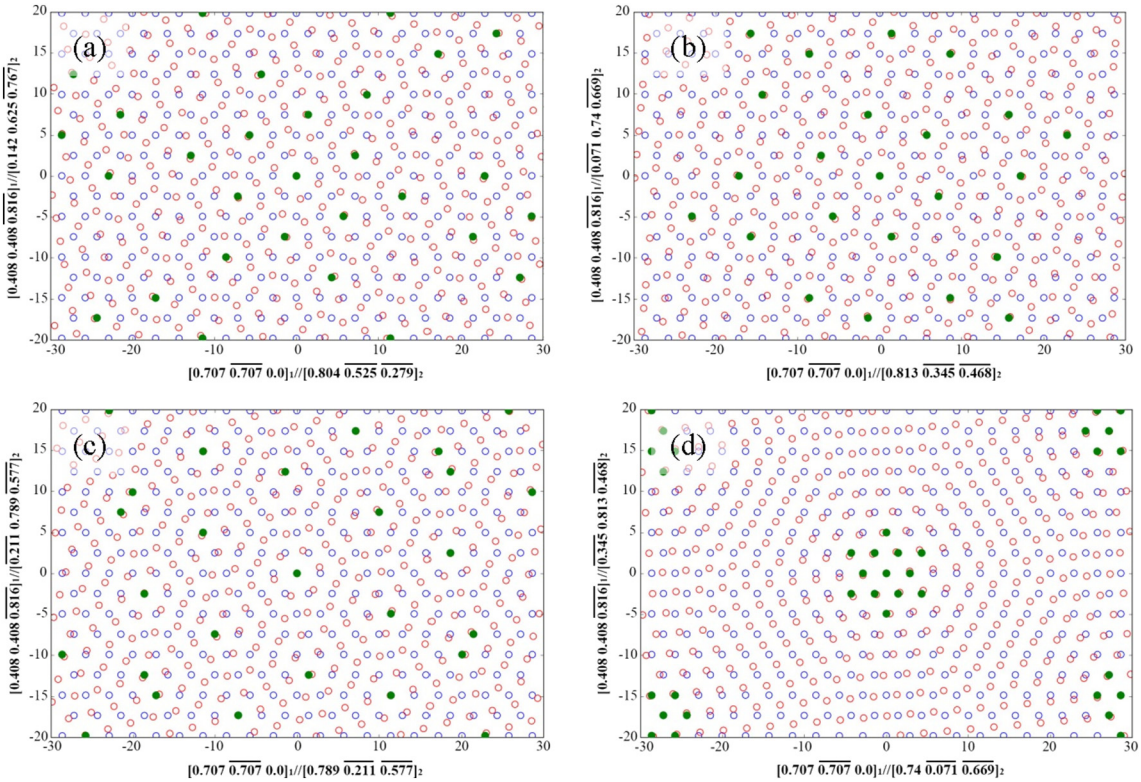


**Fig. 11.** Schematic illustrations of atomic structure of some {1 1 1}/{1 1 1} GBICs relevant to ⟨1 1 1⟩ GB component. (a) [1 1 1]/20°, (b) [1 1 1]/35°, (c) [1 1 1]/45°, (d) [1 1 1]/55°. Red and blue circles are atoms in the two abutting planes, green balls are near coincidence sites (NCS) under the conditions of NCS criterion setting to be 0.10 lattice space. (For interpretation of the references to color in this figure legend, the reader is referred to the web version of this article.)

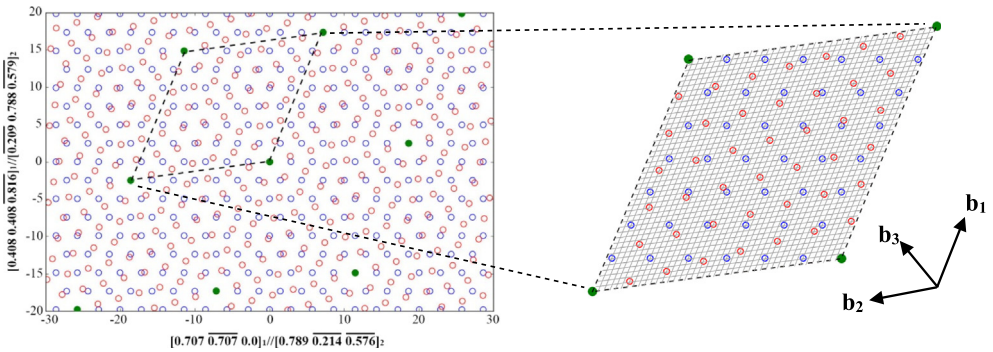


**Fig. 12.** Schematic illustrations of atomic structures of the reference state (Σ43) and its DSCL. Red and blue circles are atoms in the two abutting planes, green balls are near coincidence sites (NCS) under the conditions of NCS criterion setting to be 0.04 lattice space, $\mathbf{b}_1$, $\mathbf{b}_2$, and $\mathbf{b}_3$ are the smallest translation vector of DSCL and they are the possible Burgers vector of the dislocations of [1 1 1]/45° grain boundaries. (For interpretation of the references to color in this figure legend, the reader is referred to the web version of this article.)

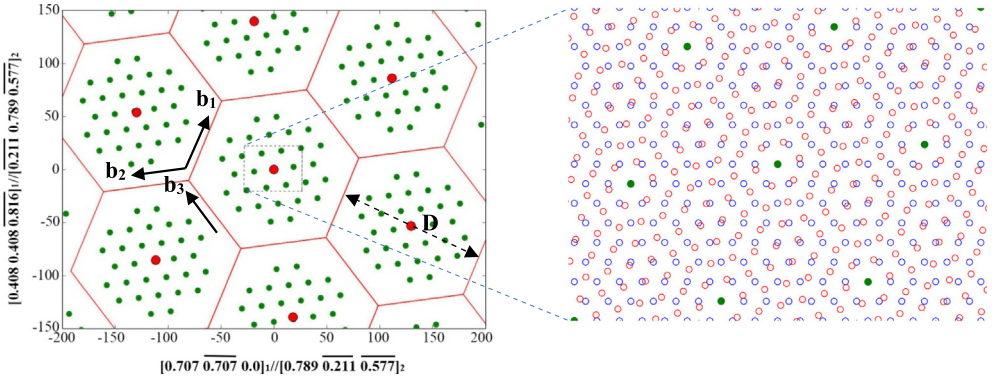


**Fig. 13.** O-lattice and dislocation configurations in the (1 1 1)/(1 1 1) GBIC of [1 1 1]/45° grain boundary. Red balls are O points, green balls are the good matching sites (GMS), Red and blue circles are atoms in the two abutting planes. (For interpretation of the references to color in this figure legend, the reader is referred to the web version of this article.)

**Table 4**
The interfacial dislocations in (1 1 1) plane with misorientation of [1 1 1]/45°.

| No. | Burgers vector | Orientation of dislocation line | Dislocation spacing D (nm) | Angle between Burgers vector and dislocation line |
|---|---|---|---|---|
| 1 | $\mathbf{b_1}$ = [6 1 −7]/86 | [0.6478 0.1065 −0.7543] | 14 | 0.081° |
| 2 | $\mathbf{b_2}$ = [−7 6 1]/86 | [−0.7543 0.6478 0.1065] | 14 | 0.081° |
| 3 | $\mathbf{b_3}$ = [−1 7 −6]/86 | [−0.1065 0.7543 −0.6475] | 14 | 0.081° |

orientation is [1 1 1]/44.82° for Σ43 and it is the reference state for figuring the dislocation structure in this GBIC. According to CSL/DSCL (Displacement complete shift lattice) theory [45,67], the smallest translation vector of DSCL are possible Burgers vector for dislocations, because these vectors will keep the CSL pattern invariant. The atomic structures of the reference state (Σ43) and the DSCL are given in Fig. 12 in which the NCS criterion is set to be 0.04a. The basis of DSCL are [0.06976 0.01162 −0.08138], [−0.08138 0.06976 0.01162] and [1 1 1], respectively. Based on the misorientation of [1 1 1]/45°, the actual deviation from the ideal matching (reference state), i.e. transformation strain, can be calculated as [68,69]:

$$\mathbf{A} = \begin{bmatrix} 1.0 & 0.00182 & -0.00181 \\ -0.00181 & 1.0 & 0.00182 \\ 0.00182 & -0.00181 & 1.0 \end{bmatrix} \tag{8}$$

According to the O-lattice theory, the principle O-lattice vector $\mathbf{X}^O$, the center of good matching site (GMS) cluster or O-point, can be calculated from

$$\mathbf{T}\mathbf{X}^O = \mathbf{b} \tag{9}$$

where $\mathbf{T} = \mathbf{I} - \mathbf{A}^{-1}$ is the displacement matrix and $\mathbf{b}$ are the Burgers vectors. Since we calculate the interfacial structure in the (1 1 1) plane, the possible translation DSCL vectors are [6 1 −7]/86, [−7 6 1]/86 and their combination [−1 7 −6]/86. The calculated O lattice is superimposed in Fig. 13 with filled big red circle. All the O-points are the center of GMS clusters. Next, the dislocation spacing will be determined for the interface. The dislocation line is given by [70]:

$$\boldsymbol{\xi}_\mathbf{i} = \boldsymbol{n} \times \boldsymbol{c}_\mathrm{i}^0 \tag{10}$$

where $\mathbf{n}$ is unit interface normal, the normal of O-cell wall is $\boldsymbol{c}_\mathrm{i}^{\,0} = \mathbf{T}'\boldsymbol{b}_\mathrm{i}^{\,*}$ and $\boldsymbol{b}_\mathrm{i}^{\,*} = \boldsymbol{b}_\mathrm{i}^{\,\mathrm{L}}/|\boldsymbol{b}_\mathrm{i}^{\,\mathrm{L}}|^2$. The dislocation spacing is given by [70]:

$$\mathrm{D_i} = 1/|\boldsymbol{\xi}_\mathrm{i}| \tag{11}$$

The calculated results for three Burgers vectors are shown in Table 4. They are all screw dislocations and dislocation spacing D is around 14 nm. The dislocation configurations or networks in the (1 1 1)/(1 1 1) GBIC of [1 1 1]/45° is shown by red lines in Fig. 13. The local magnification (dotted line framed area in Fig. 13) which shows the atomic structure of (1 1 1)/(1 1 1) GBIC of [1 1 1]/45° in detail with a NCS criterion setting to be 0.04a is given in the right of Fig. 13.

It is clear that, in addition to its higher PCSD, (1 1 1)/(1 1 1) GBIC with a given misorientation of [1 1 1]/45° has definite dislocation structures comparing to the general GBs, and these dislocation structures can be rationalized by CSL/DSCL theory. Same results can be obtained when same analyses are applied to the other (1 1 1)/(1 1 1) GBICs with misorientations rotated around [1 1 1] for varied angles, such as [1 1 1]/20°, [1 1 1]/35°, [1 1 1]/55° and so on. Such features may be closely related to the structure stability and, or in other words, the {1 1 1}/{1 1 1} GBICs observed in present work may possess higher structural stability and it could be the reason for their sluggish mobility compared to the general GBs observed by Janssens et al. [63]. This result implies that, apart from the coherent twin boundaries of very limited frequency, to pursue other {1 1 1}/{1 1 1} GBICs as high frequent as possible is a pint-cut for the GBE research and applications in the high SFE FCC materials.

## 5. Conclusions

The GBICs in a multi-directional forged and recrystallized high purity aluminum, whose crystallographic textures can be neglected (random orientation) have been investigated by EBSD measurement and stereology-based FPA coupled with crystallographic analysis. Some conclusions can be drawn as following

(1) The GBICs for any group of GBs with a given misorientation are not random, showing remarkable preference on the planes of low Miller index forming mixed and twist GBs.
(2) Among the HABs, {1 1 1}/{1 1 1} including coherent Σ3 boundaries is the most frequent GBIC, mainly coming from the GBs formed by rotations around ⟨1 1 1⟩, ⟨1 2 2⟩ and ⟨1 1 2⟩ axes.
(3) The {1 1 1}/{1 1 1} GBICs usually possesses higher planar coincidence site density (PCSD) and definite dislocation structures compared to the general GBs, implying their more structural stability if only crystallography is considered.
(4) Apart from the coherent twin boundaries, to pursue other {1 1 1}/{1 1 1} GBICs as high frequent as possible may be a pint-cut for the GBE research and applications in the high SFE FCC materials.

## Acknowledgements

This work was supported by National Natural Science Foundation of China under the contract Nos. 51171095 and 51271058. The authors sincerely thank professor Wenzheng Zhang from Tsinghua University for her helpful suggestions and discussions concerning the O-lattice theory and its applications in current work.

## References


[1] K.T. Aust, J.W. Rutter, Grain boundary migration in high purity lead and dilute lead-tin alloys, Trans. AIME 215 (1959) 119–125.
[2] M.N. Kelly, K. Glowinski, N.T. Nuhfer, G.S. Rohrer, The five parameter grain boundary character distribution of α-Ti determined from three-dimensional orientation data, Acta Mater. 111 (2016) 22–30.
[3] F.C. Frank, Symposium on the Plastic Deformation of Crystalline Solid, Pittsburgh, PA Office of Naval Research, 1950.
[4] B.A. Bilby, R. Bullough, E. Smith, Continuous distributions of dislocation: a new application of the methods of non-Riemannian geometry, Proc. Roy. Soc. 231 (1955) 261–269.
[5] A. Yamanaka, K. McReynolds, P.W. Voorhees, Phase field crystal simulation of grain boundary motion, grain rotation and dislocation reactions in a BCC bicrystal, Acta Mater. 133 (2017) 160–171.
[6] L. Yang, S.Y. Li, A modified synthetic driving force method for molecular dynamics simulation of grain boundary migration, Acta Mater. 100 (2015) 107–117.
[7] M.L. Kronber, F.H. Wilson, Secondary recrystallization in copper, Trans. AIME 185 (1949) 501–514.
[8] D. Wolf, S. Yip, Materials Interfaces, Chapman & Hall, London, 1992.
[9] T. Watanabe, An approach to grain boundary design for strong and ductile polycrystal, Res. Mechanics 11 (1984) 47–52.
[10] B.L. Adams, S.I. Wright, K. Kunze, Orientation imaging: the emergence of a new microscopy, Metall. Trans. A 24 (1993) 819–830.
[11] M. Shimada, H. Kokawa, Z.J. Wang, Y.S. Sato, I. Karibe, Optimization of grain boundary character distribution for intergranular corrosion resistant 304 stainless steel by twin-induced grain boundary engineering, Acta Mater. 50 (2002) 2331–2341.
[12] H.Y. Bi, H. Kokawa, Suppression of chromium depletion by grain boundary structural change during twin-induced grain boundary engineering of 304 stainless steel, Scr. Mater. 49 (2003) 219–223.
[13] F.X. Fang, K. Zhang, H. Guo, W.G. Wang, B.X. Zhou, Twin-induced grain boundary engineering in 304 stainless steel, Mater. Sci. Eng. A 487 (2008) 7–13.
[14] G. Palumbo, U. Erb, Enhancing the operating life and performance of lead-acid batteries via grain-boundary engineering, MRS Bull. 11 (1999) 27–32.
[15] W.G. Wang, F.X. Yin, H. Guo, H. Li, B.X. Zhou, Effects of recovery treatment after large strain on the grain boundary character distributions of subsequently cold rolled and annealed Pb–Ca–Sn–Al alloy, Mater. Sci. Eng. A 491 (2008) 199–206.
[16] W.G. Wang, B.X. Zhou, G.S. Rohrer, H. Guo, Z.X. Cai, Textures and grain boundary character distributions in a cold rolled and annealed Pb-Ca based alloy, Mater. Sci. Eng. A 527 (2010) 3695–3706.
[17] P. Lin, G. Palumbo, U. Erb, K.T. Aust, Influence of grain boundary character distribution on sensitization and intergranular corrosion of alloy 600, Scr. Metall. Mater. 33 (1995) 1387–1392.
[18] S. Xia, B.X. Zhou, W.J. Chen, W.G. Wang, Effects of strain and annealing processes on the distribution of Σ3 boundaries in a Ni-based superalloy, Scr. Mater. 54 (2006) 2019–2022.
[19] S. Xia, B.X. Zhou, W.J. Chen, Grain cluster microstructure and grain boundary character distribution in alloy 690, Metall. Mater. Trans. A 40 (2009) 3016–3033.
[20] V. Randle, The influence of annealing twinning on microstructure evolution, J. Mater. Sci. 40 (2005) 853–859.
[21] V. Randle, Y. Hu, The role of vicinal Σ3 boundaries and Σ9 boundaries in grain boundary engineering, J. Mater. Sci. 40 (2005) 3243–3246.
[22] G. Palumbo, K.T. Aust, On annealing twins and CSL distributions in F.C.C. polycrystals, Phys. Status Solidi A 131 (1992) 425–428.
[23] V. Randle, Mechanism of twinning-induced grain boundary engineering in low stacking-fault energy materials, Acta Mater. 47 (1999) 4187–4196.
[24] F.J. Humphreys, M. Hatherly, Recrystallization and Related Annealing Phenomenon, 2nd edition, Elsevier Ltd., Oxford, 2004.
[25] W.H. Yin, W.G. Wang, X.Y. Fang, In-situ observations on the annealing behavior of triple junctions in a high purity nickel after slight cold rolling, Sci. Sin. Tech. 47 (2017) 1189–1197.
[26] W.G. Wang, C. Lin, G.H. Li, N.B. Hua, B.X. Zhou, X.Y. Fang, P.Q. Dai, W.Z. Chen, Preferred orientation of grain boundary plane in recrystallized high purity aluminum, Sci. Sin. Tech. 44 (2014) 1295–1308.
[27] V. Randle, Special boundaries and grain boundary plane engineering, Scr. Mater. 54 (2006) 1011–1015.
[28] W.G. Wang, Y. Dai, J.H. Li, B.X. Liu, An atomic-level mechanism of annealing twinning in copper observed by molecular dynamics simulation, Cryst. Growth Des. 11 (2011) 2928–2934.
[29] W.G. Wang, S. Chen, G.S. Rohrer, W.Z. Chen, The inter-connections of Σ3 boundaries in pure iron, Scr. Mater. 128 (2017) 18–22.
[30] D.N. Dunn, G.J. Shiflet, R. Hull, Quantitative three-dimensional reconstruction of geometrically complex structures with nanoscale resolution, Rev. Sci. Instrum. 73 (2002) (330-312).
[31] A.D. Rollett, S.B. Lee, R. Campman, G.S. Rohrer, Three-dimensional characterization of microstructure by electron back-scatter diffraction, Annu. Rev. Mater. Res. 37 (2007) 627–658.
[32] G.S. Rohrer, D.M. Saylor, B.E. Dasher, B.L. Adams, A.D. Rollett, P. Wynblatt, The distribution of internal interfaces in polycrystals, Z. Metall. 95 (2004) 197–214.
[33] D.M. Saylor, B.E. Dasher, B.L. Adams, G.S. Rohrer, Measuring the five-parameter grain-boundary distribution from observation of planar sections, Metall. Mater. Trans. A 35 (2004) 1981–1989.
[34] P.H. Pumphrey, A plane matching theory of high angle grain boundary structure, Scr. Metall. 6 (1972) 107–114.
[35] V. Randle, B. Ralph, The coincident axial direction (CAD) approach to grain boundary structure, J. Mater. Sci. 23 (1988) 934–940.
[36] G. Palumbo, K.T. Aust, A coincident axial direction (CAD) approach to the structure of triple junctions in polycrystalline materials, Scr. Metall. 24 (1990) 1771–1776.
[37] E. Tochigi, Y. Kezuka, N. Shibata, A. Nakamura, Y. Ikuhara, Structure of screw dislocations in a (0001)/[0001] low-angle twist grain boundary of alumina (a-$Al_2O_3$), Acta Mater. 60 (2012) 1293–1299.
[38] A.P. Sutton, R.W. Balluffi, Interfaces in Crystalline Materials, Clarendon Press, Oxford, 1995.
[39] Y. Buranova, H. Rosner, S.V. Divinski, R. Imlau, G. Wilde, Quantitative measurements of grain boundary excess volume from HAADF-STEM micrographs, Acta Mater. 106 (2016) 367–373.
[40] A.D. Banadaki, S. Patala, A simple faceting model for the interfacial and cleavage energies of Σ3 grain boundaries in the complete boundary plane orientation space, Comput. Mater. Sci. 112 (2016) 147–160.
[41] P.R. Cantwell, M. Tang, S.J. Dillon, J. Luo, G.S. Rohrer, M.P. Harmer, Grain boundary complexions, Acta Mater. 62 (2014) 1–48.
[42] W.E. Frazier, G.S. Rohrer, A.D. Rollett, Abnormal grain growth in the Potts model incorporating grain boundary complexion transitions that increase the mobility of individual boundaries, Acta Mater. 96 (2015) 390–398.
[43] J.Y. Nie, J.M. Chan, M.D. Qin, N.X. Zhou, J. Luo, Liquid-like grain boundary complexion and sub-eutectic activated sintering in CuO-doped $TiO_2$, Acta Mater. 130 (2017) 329–338.
[44] W. Bollmann, Crystal Defects and Crystalline Interfaces, Springer, Berlin, 1970.
[45] W. Bollmann, O-lattice calculation of an F.C.C.-B.C.C. interface, Phys. Status Solidi A 21 (1974) 543–550.
[46] G.S. Rohrer, J. Li, S. Lee, A.D. Rollett, M. Groeber, M.D. Uchic, Deriving the grain boundary character distribution and relative grain boundary energies from three dimensional EBSD data, Mater. Sci. Technol. 26 (2010) 661–669.
[47] J.L. Wang, R. Janisch, G.K.H. Madsen, R. Drautz, First-principles study of carbon segregation in bcc iron symmetrical tilt grain boundaries, Acta Mater. 115 (2016) 259–268.
[48] J.K. Mackenzie, Second paper on statistics associated with the random disorientation of cubes, Biometrika 45 (1958) 229–240.
[49] V. Randle, O. Engler, Introduction to Texture Analysis: Macrotexture, Microtexture and Orientatiuon Mapping, Gordon and Breach Science, Amsterdam, 2000.
[50] F.C. Frank, Orientation mapping, Metall. Trans. A 19 (1987) 403–408.
[51] W.G. Wang, Y. Lin, P.Q. Dai, G.S. Rohrer, W.Z. Zhang, Grain boundary plane distributions in a cold rolled and annealed high purity iron, Mater. Charact. 122 (2016) 6–13.
[52] X.Y. Huang, The Microstructure of Materials and Its Electron Microscopy Analysis, Metallurgical Industry Press, Beijing, 2008.
[53] J. Li, S.J. Dillon, G.S. Rohrer, Relative grain boundary area and energy distributions in nickel, Acta Mater. 57 (2009) 4304–4311.
[54] F.C. Frank, Growth and Perfection of Crystals, John Wiley, New York, 1958.
[55] J. Lind, S.F. Li, M. Kumar, Twin related domains in 3D microstructures of conventionally processed and grain boundary engineered materials, Acta Mater. 114 (2016) 43–53.
[56] S. Irukuvarghula, H. Hassanin, C. Cayron, M.M. Attallah, D. Stewart, M. Preuss, Evolution of grain boundary network topology in 316L austenitic stainless steel during powder hot isostatic pressing, Acta Mater. 133 (2017) 269–281.
[57] C. Shen, J. Li, Y.Z. Wang, Predicting structure and energy of dislocations and grain boundaries, Acta Mater. 74 (2014) 125–131.
[58] G.J. Tucker, M.A. Tschopp, D.L. McDowell, Evolution of structure and free volume in symmetric tilt grain boundaries during dislocation nucleation, Acta Mater. 58 (2010) 6464–6473.
[59] W.G. Wang, B.X. Zhou, L. Feng, X. Zhang, S. Xia, Grain boundary character distributions (GBCD) of cold rolled Pb-Ca-Sn-Al alloy during recovery and recrystallization, Acta Metall. Sin. 42 (2006) 715–721.
[60] W.G. Wang, H. Guo, Effects of thermo-mechanical iterations on the grain boundary character distribution of Pb-Ca-Sn-Al alloy, Mater. Sci. Eng. A 445–446 (2007) 155–162.
[61] K. Zhang, W.G. Wang, X.Y. Fang, H. Guo, Grain boundary character distributions of Pb–Ca–Sn–Al alloy annealed at elevated temperature after rolling at different temperatures, Acta Metall. Sin. 44 (2008) 652–658.
[62] X.Y. Fang, Z.Y. Liu, M. Tikhonova, A. Belyakov, W.G. Wang, Evolution of texture and development of $\Sigma 3^n$ grain clusters in 316 austenitic stainless steel during thermal mechanical processing, J. Mater. Sci. 48 (2013) 997–1004.
[63] K.G.F. Janssens, D. Oolmsted, E.A. Holm, S.M. Foiles, S.J. Plimpton, P.M. Derlet, Computing the mobility of grain boundaries, Nat. Mater. 5 (2006) 124–127.
[64] D. Bouchet, L. Priester, Grain boundary plane and intergranular segregation in nickel-sulfur system, Scr. Metall. 21 (1987) 475–478.
[65] D. Bouchet, B. Aufray, L. Priester, Experimental evidence of sulfur effect on the plane and on the extrinsic dislocations of a sigma 3 grain boundary in nickel, J. Phys. 49 (1988) C5–417.
[66] Q. Liang, W.T. Reynolds, Determining interphase boundary orientations from near-coincidence sites, Metall. Mater. Trans. A 29 (1998) 2059–2072.
[67] H. Grimmer, W. Bollmann, D.H. Warrington, Coincidence-site lattices and complete pattern-shift lattices in cubic crystals, Acta Crystallogr. Sect. A: Cryst. Phys., Diffr., Theor. Gen. Crystallogr. 30 (1974) 197–207.
[68] F. Ye, W.Z. Zhang, Coincidence structures of interfacial steps and secondary misfit dislocations in the habit plane between Widmanstatten cementite and austenite, Acta Mater. 50 (2002) 2761–2777.
[69] W.Z. Zhang, G.C. Weatherly, On the crystallography of precipitation, Prog. Mater. Sci. 50 (2005) 181–292.
[70] W.Z. Zhang, Formulas for periodic dislocations in general interfaces, Appl. Phys. Lett. 86 (2005) 1219–1222.